Energy loss in large-angle scattering of slow, highly charged Ar ions from a Au surface

W. Huang, H. Lebius, and R. Schuch*
Department of Atomic Physics, Stockholm University, S-104 05 Stockholm, Sweden

M. Grether and N. Stolterfoht
Hahn-Meitner-Institut, Glienicker Strasse 100, D-14109 Berlin, Federal Republic of Germany
(Received 13 March 1998)

Energy loss of slow ($v \approx 0.06$ a.u.), highly charged Ar^{9+} ions scattered from a Au(111) single-crystal surface has been investigated for different incident angles ($\psi = 5°$ and 37.5°) and a fixed scattering angle of 75°. The energy position of the elastic peak agrees well with the value expected for the binary elastic scattering. At small incidence angle (5°) an additional inelastic energy loss was identified in spite of the large scattering angle. This additional energy loss is found to compare well with a combination of a modified Firsov model with processes of electron capture, recapture, Auger transitions, and image charge acceleration during the ion-surface interactions. [S1050-2947(98)09609-7]

PACS number(s): 34.50.Dy, 79.20.Rf

I. INTRODUCTION

The interaction of slow, highly charged ions (HCIs) with solid surfaces has been extensively studied in the past few years [1]. Information on HCI-surface interactions was mainly obtained by measuring the emitted electrons [1–3] and x rays [1,4,5]. Some measurements of the angular distributions and the final charge-state distributions of the scattered ions in small angles [6–11] and in large angles [12,13] were done. Information on HCI-surface interactions may also be obtained from the energy loss occurring in transmission [14,15] and scattering of ions [16,17]. Since energy loss, especially inelastic energy loss, depends mainly on the processes of electron capture and recapture, electron excitation, and surface and bulk plasmon excitation, the measurement of energy loss can therefore provide additional information on the neutralization during the HCI-surface interaction.

The measurements of energy loss of HCI provide, however, only integral information on the whole interaction of the projectile along its trajectory with atoms on the surface. The situation gets somewhat clearer for large-angle scattering, since the ion is scattered by one or two atoms on the surface [12,13] and the energy loss is almost exclusively due to kinematics and almost independent of charge-exchange processes [18]. In the case when the ion approaches the surface at a small angle, it is scattered by many atoms on the surface in more distant interactions. Electron flux from the atoms in the solid and the valence and conduction bands occurs into different n states of the ion. The friction due to the acceleration into the ion moving frame can cause measurable energy loss [16]. Only a few studies of inelastic energy loss of HCIs have been reported in the literature for transmission [14,15] and scattering [16,17]. These scattering studies were carried through in grazing-angle geometry and it was demonstrated that the inelastic energy loss of scattered ions disappears with increasing scattering angles and decreasing velocities. Another finding in these studies is a weak influence of the initial charge state of the projectile on the energy loss [16,17]. This is interpreted by a full neutralization of the projectile on the incoming trajectory to the surface [16].

In the present experiment we found measurable inelastic energy loss also for large scattering angles when the incident angle was small. This was the case even for very low incident velocities. We studied also the relationship between the degree of neutralization, i.e., the final charge state and the energy loss when the HCIs scatter from the surface. By varying incident angle and analyzing the energy loss of the scattered ions accurately we can decompose the contributions of the energy loss from different mechanisms such as single binary scattering, double binary scattering and inelastic processes. The experimental results will be quantitatively interpreted by combining the modified Firsov model with a model calculation that takes into account the processes of electron capture, recapture, and Auger transitions. This shows in the case of a small incident and large exit angle that the inelastic energy loss mainly stems from the incoming trajectory of the ion. The interaction time gets short and therefore the inelastic energy loss small when the ion leaves the surface at large angle. In particular, we found that the inelastic energy loss of the scattered ions can be mainly ascribed to the contributions of the valence electrons of atoms in high-n states and the inner-shell populations of the ion, which are strongly dependent on the neutralization processes during the ion-surface interactions. Atomic units are used throughout in this paper, unless otherwise specified.

II. EXPERIMENTAL METHOD

The experiments were performed using the 14-GHz Electron Cyclotron Resonance ion source facility at the Hahn-Meitner-Institute in Berlin. The ion source provides ions with energies up to $20q$ keV (where q is the charge state of the extracted ions). The beam line is equipped with a deceleration lens system. After a charge-state analysis and beam transportation, the ions were decelerated to final energies of 4 keV ($v \approx 0.06$ a.u.), keeping the experimental setup on the ground potential. The essential parts of experimental setup for low-energy ion scattering spectroscopy include an ion

*Author to whom correspondence should be addressed. Electronic address: Schuch@msi.se

sputter gun, a low-energy electron diffraction (LEED) system, and a tandem parallel-plate electrostatic analyzer [19]. The analyzer can be rotated $0°-135°$ with respect to the primary beam direction and it can also be adopted to perform the high-resolution Auger spectroscopy. A more detailed description of the system can be found elsewhere [20].

The Au(111) single crystal was mounted on an x-y-z-ψ-ϕ manipulator located in the ultrahigh vacuum chamber with a base pressure of 5×10^{-10} mbar. The crystal quality was controlled by a LEED system. The crystal surface was prepared by repeating cycles of sputtering and annealing. The cleanliness was verified by means of electron-induced Auger spectroscopy. The surface remained clean during the measurement due to the high incident ion current, typically 100 nA. The beam current measured on the target was taken for on-line normalization.

The Ar^{9+} beam was collimated to a diameter of about 2 mm and was directed onto the crystal surface with incident angles $\psi=5°$ and 37.5°. The crystal was aligned in a planar channeling direction with respect to the Au(011) crystallographic plane. The primary beam energy was calibrated by directly passing the primary beam through the analyzer. The variation of the primary beam energy caused by the instability of the source plasma is less than a few eV. A systematic error in the energy calibration should be of the same order. For the measured energy loss this error plays a minor role. In the plots and tables statistical error bars are given. The azimuthal orientation was determined by measuring the yield of scattered ions as a function of the azimuthal angle ϕ. Scattered particles were detected at an angle of $\theta=75°$.

The acceptance angle of the analyzer was about 1° and it had an overall energy resolution of about 5×10^{-2}. In order to ensure high-resolution measurements, a set of high-quality power supplies with mV accuracy were used for the analyzer. The energy width of scattered particles due to the finite acceptance angle is small compared to the overall resolution. The ions selected by the analyzer were detected by means of a channeltron detector. Another channeltron detector was positioned at the back of the analyzer to measure the neutral particles that passed through a hole on the outer plate of the analyzer.

III. RESULTS

Figure 1 shows six typical kinetic-energy spectra obtained from a primary beam of Ar^{9+} incident at $\psi=37.5°$ and 5°, scattered into the same detection angle of $\theta=75°$ (inset of Fig. 1). The spectra with $Q=+1$, $+2$, and $+3$ correspond to Ar ions leaving the surface in single, double, and triple ionized states, respectively. They are transformed into the same energy scale by multiplying the spectrometer voltage with the spectrometer constant and Q. Particularly for $\psi=5°$ the spectra for higher Q have a background on their high energy-side from the low-energy tail of the $Q-1$ spectrum, due to a large variation of the intensities.

The arrows marked by E_{kin} indicate the calculated kinetic energies by assuming a single binary Ar-Au collision [formula (2) in Sec. IV], while the arrow marked E_0 denotes the primary beam energy. In the cases of large incident angle $\psi=37.5°$ (see the upper diagram in Fig. 1) a relative yield of neutralization was found to be around 65%. The kinetic-

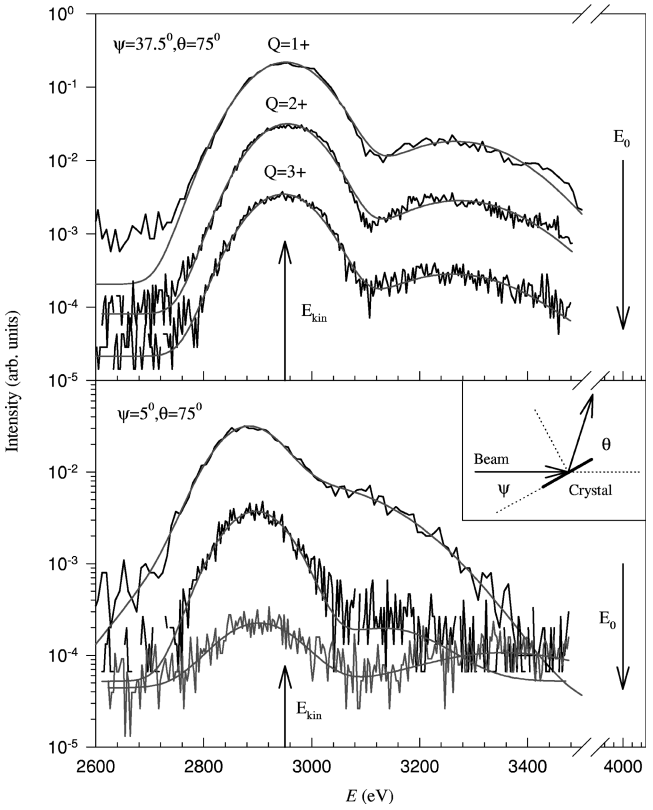

FIG. 1. Energy spectra of 4-keV Ar^{9+} ions scattered from a Au(111) surface with incident angles of $\psi=37.5°$ (top diagram), $\psi=5°$ (bottom diagram), and the scattering angle of $\theta=75°$. E and Q denote the energy and final charge states of scattered ions, respectively. E_0 and E_{kin} are the primary beam energy and the energy of the scattered ions calculated by kinematics assuming single Ar-Au collisions (marked by arrows), respectively. The solid lines represent the fits to the data by Gaussians and the inset shows the scattering geometry.

energy spectra for each outgoing charge states consists of a two-peak structures: a main peak and a quite well resolved small peak or a shoulder at higher energies side. One finds that the main peak in the spectra is very well aligned with the E_{kin} mark. This indicates that the energy loss can be predominately attributed to the momentum transfer between the ion and a single Au atom on the surface. According to a Marlowe simulation of scattering trajectories [21], the peak at higher energy can be ascribed by two sequential binary collisions at two neighboring Au atoms with scattering angles $\theta_1+\theta_2=75°$, e.g., a sequence of two collisions with $\theta_1=18°$ and $\theta_2=57°$ in the case of $\psi=25°$.

In order to extract some detailed information from Fig. 1, a least-squares fitting procedure is carried through to deconvolute the spectra. Here it is assumed that the spectra can be deconvoluted into three main contributions: single collisions, double collisions, and noise background. The spectral distribution of scattered ions is assumed to be a superposition of Gaussians. A constant background is used in the fitting procedure. The quality of the fitting curves are evaluated by the so-called χ^2 test, i.e., searching for $\chi^2\approx1$. The fitting curves are included in Fig. 1 (solid lines) to compare with the observed data. The fitting parameters are summarized in Table I and they will be discussed in the forthcoming sections. The error bars given are due to statistics.

TABLE I. Fitting results for the scattered Ar^{Q+} ions as shown in Fig. 1, where E_1 and E_2 represent the energetic positions of the peaks for single and double scatterings, respectively. Here the E loss is equal to E_0-E_1 (where E_0 is the primary beam energy).

Q	E_1 (eV)	E_2 (eV)	χ^2	E loss (eV)
		$\psi=37.5°,\ \theta=75°$		
1+	2951.4±0.4	3265.5±2.6	3.3	1048.6±0.4
2+	2954.7±0.3	3272.8±1.8	3.4	1045.3±0.3
3+	2947.4±0.6	3261.0±2.6	1.4	1052.6±0.6
		$\psi=5°,\ \theta=75°$		
1+	2880.4±1.2	3002.3±5.1	0.9	1119.6±1.2
2+	2895.9±1.4	3135.7±19.7	1.1	1104.1±1.4
3+	2902.0±3.7	3356.9±20.0	1.1	1098.0±3.7

For a $\psi=5°$ incident angle (see the bottom diagram in Fig. 1), a higher degree of neutralization (around 90%) was observed. The decreasing fraction of charged, scattered particles relative to the neutralized particles is not very surprising as a decreasing incident angle increases the interaction time and the number of close interactions that may lead to more efficient neutralization when the ion approaches the surface. At a close inspection one finds two interesting phenomena: first, the main peak is at a lower energetic position than that calculated by kinematics of single binary scattering (see the mark in Fig. 1) and second, the double-scattering peak is not as well resolved as at larger incidence angles and almost disappears. The first point indicates that an additional energy loss due to inelastic processes may be involved. It is very likely that the Ar ions observed at $\psi=5°$ and $\theta=75°$ stem from collisions at surface steps or other surface imperfections. We considered then the possibility that the energy shift of the single collision peak is due to projectiles that have partially penetrated the surface at such step edges before being scattered. However, these would experience a largely varying additional inelastic energy loss from different penetration depths. The peaks at $\psi=5°$ would thus be smeared out. They would be considerably broader than the peaks at $\psi=37.5°$, which is not the case. This was therefore excluded as an obvious reason for the additional energy shift and we assume the Ar ions at $\psi=5°$ scatter at single Au atoms like in the case of $\psi=37.5°$ but have different trajectories relative to the surface that are treated below.

To the second point of a vanishing double-scattering peak, we found in previous investigations [21] that the yield and the energetic position of a double collision can change drastically, depending on the scattering trajectories and crystal orientation. The intensity of the double-scattering peak was strongest in channeling direction. Scattering at large outgoing angles and small incoming angles could occur predominantly at dislocations or steps in the surface. Double scattering could thus be reduced at small incidence angles.

IV. MODEL CALCULATIONS

In order to give further insight into the energy loss of HCIs at surfaces and to give a quantitative interpretation of experimental results a model simulation was carried out. The model assumes that the total energy loss E_{total} that ions experience along their trajectory can be decomposed into three major contributions, i.e.,

$$E_{total}=E_{el}+E_{in}-E_{im}, \tag{1}$$

where E_{el} stands for elastic energy loss, E_{in} inelastic energy loss, and E_{im} the image charge energy gain.

For scattering, the interaction time Δt is typically $\Delta t \approx b/v$ (b being the impact parameter, e.g., $b\approx 1$ a.u. at the distance of closest approach). Thus Δt is on the order of femtoseconds, which is much shorter than the vibration time (picoseconds) of the target atoms. The transfer of energy to the target atom thus is much larger than the binding energy of the atoms to the crystal lattice. The Au target atoms behave as if they were free. Here the elastic energy loss E_{el} is described by the kinetic energy E_{kin} assuming a single binary ion-atom collision. E_{el} can therefore be expressed by the formula [22]

$$E_{kin}=E_0\left(\frac{\cos\theta\pm\sqrt{(\mu^2-\sin^2\theta)}}{1+\mu}\right)^2,$$

$$E_{el}=E_0-E_{kin}, \tag{2}$$

where E_0 is the initial energy of the projectile $\mu=m_t/m_p$ (m_p and m_t are the mass of the projectile and target atom). The choice of the minus sign in Eq. (2) holds only for $m_p>m_t$, whereas for $m_p\leqslant m_t$ only the plus sign may be applied. In the present studies, one gets $E_{el}=1050$ eV for the detection angle of $\theta=75°$ using expression (2).

The amount of the image-charge energy gain E_{im} in expression (1) is directly related to the degree of neutralization and to the distances where electron capture occurs [23–25]. In the present study, the energy gain E_{im} for different outgoing charge states Q is evaluated by the classical over-barrier model [24] assuming a staircaselike charge-state evolution from q to Q:

$$E_{im}(Q)=\frac{q^2}{4d_1}+\sum_{j=1}^{q-(1+Q)}\frac{(q-1)^2}{4}\left(\frac{1}{d_j}-\frac{1}{d_{j+1}}\right),$$

$$d_j\approx\frac{\sqrt{2(q-j+1)}}{W}, \tag{3}$$

where d_j is the distance where step j in the staircaselike charge transfer takes place. W is the work function of Au. An evolution of the charge state via a complete neutralization back to Q would not change $E_{im}(Q)$ noticably.

Because of the image attraction the ion is accelerated on the incident path and decelerated by a decreasing amount on the outgoing path, depending on the degree of neutralization. The gain in velocity perpendicular to the surface leads to a bending of ion trajectory towards the surface and results in an increased effective scattering angle [26] $\theta+\Delta\theta_{im}$,

$$\Delta\theta_{im}=\sin^{-1}\left[\left(\sin^2\psi+\frac{E_{im}}{E_0}\right)^{1/2}\right]-\psi. \tag{4}$$

Since elastic energy loss E_{el} depends on the scattering angle θ [see expression (2)] it has to be corrected as well by re-

TABLE II. Energy loss calculated in terms of elastic energy loss E_{el}, the corrected elastic energy loss E_{el}^*, the image change energy gain E_{im}, the inelastic energy loss E_{in} (see the text), and $E_{total}=E_{el}^*+E_{in}-E_{im}$.

Q	E_{el} (eV)	E_{el}^* (eV)	E_{im} (eV)	E_{in} (eV)	E_{total} (eV)
		$\psi=37.5°,\ \theta=75°$			
1+	1050	1058	27	13	1044
2+	1050	1058	27	13	1044
3+	1050	1058	26	13	1045
		$\psi=5°,\ \theta=75°$			
1+	1050	1089	27	58	1120
2+	1050	1088	27	58	1119
3+	1050	1088	26	58	1120

placing θ with $\theta+\Delta\theta_{im}$. One gets the increased effective scattering angles $\Delta\theta_{im}\approx 1.85°$ for $\psi=5°$ and $\Delta\theta_{im}\approx 0.39°$ for $\psi=37.5°$, respectively.

In Table II we summarize the calculated energy loss in terms of elastic energy loss E_{el}, the corrected elastic energy loss E_{el}^* by taking into account the increased effective scattering angle, the image-charge energy gain E_{im}, the inelastic energy loss E_{in}, and the total energy loss E_{total}. To calculate the inelastic energy loss E_{in} different models have been employed in the literature (see [1,16]). Here E_{in} is calculated based on the modified Firsov model [27]. The model has been used quite successfully by Winecki *et al.* [16] to explain inelastic energy loss observed in grazing-angle scattering of Ar^{q+} on graphite. We extend the modified Firsov model by taking into account the neutralization processes when ions approach and scatter from the surface. The model for neutralization [12,13] includes processes of electron capture into Ar inner shells ($n\geqslant 3$), recapture to the surface, and Auger transitions during the ion-surface interaction. A contribution from the excitation of surface and bulk plasmons to the energy loss is neglected here.

In the modified Firsov theory, inelastic energy loss is determined for collisions with every individual atom at a given impact parameter and for the population of the different shells in the colliding partners. The model utilizes the Hartree-Fock-Slater approximation [28] to evaluate the electronic potential and to determine the contributions to the energy loss from different shells. The energy loss due to a particular shell with the principal quantum number n can be analytically expressed as [27]

$$E_{n,i}=\pi m v\frac{r}{r_i}\omega_{n,i}u_{n,i}I_{n,i}(\eta_{n,i}), \tag{5}$$

where the indices $i=1$ and 2 represent the Ar ion and Au atom, respectively; m is the electron mass, $\omega_{n,i}$ is the population in different shells for two colliding partners, and $u_{n,i}=Z_{eff}(\omega_{n,i})/n$ is the average electron velocity of the shell. $Z_{eff}(\omega_{n,i})$ is the effective nuclear charge depending on the populations in different shells, which is determined by Slater rules as shown in various handbooks, e.g., in Ref. [29]. $I_{n,i}(\eta_{n,i})$ is an integral depending on the overlap of wave functions for the shells under consideration. $\eta_{n,i}=2r_i[Z_{eff}/(\omega_{n,i})n]$ is the argument for the integral $I_{n,i}(\eta_{n,i})$ and r_i is a parameter and has to be determined later.

For small impact parameters ($p/\eta_{n,i}\geqslant 1$), the integral $I_{n,i}(\eta_{n,i})$ in Eq. (5) can be reduced to

$$I_{n,i}(\eta_{n,i})\simeq\frac{1}{2\sqrt{2\pi}}\frac{p^{p+3/2}}{\Gamma(p+2)}e^{-p}\frac{1}{\eta_{n,i}}, \tag{6}$$

where $\Gamma(p+2)$ is the Gamma function, $p=2n^*-1$, and n^* is the effective principal quantum number given by the Slater orbital [29]. In the case of large impact parameters ($p/\eta_{n,i}<1$) the integral can be expressed as an exponentially decaying function

$$I_{n,i}(\eta_{n,i})\simeq\sqrt{\frac{2\pi}{\eta_{n,i}}}e^{-\eta_{n,i}}\left(1+\frac{3p}{2\eta_{n,i}}\right). \tag{7}$$

In order to describe the electron flux that causes inelastic energy loss, a dividing surface **S** is used in the modified Firsov model. The surface **S** intersects the internuclear axis of two colliding partners where the electron density has a minimum. In other words, **S** separates the potential attraction from the two colliding partners. It is assumed that an electron will lose temporarily its initial momentum and acquire a new momentum centered around the velocity of the other particle when it passes through **S**. In such a way, the ion loses energy. The ratio r/r_i in Eq. (5) is used to characterize the fraction of r between the target atom and **S** and between the ion and **S** (where r, the distance of the ion to the surface atom, is assumed equal to the impact parameter). The values of r_i ($i=1$ and 2) are determined by the relations [30]

$$\begin{aligned}&Z_{eff1}^{3/2}\{d_1[H_1(e^{r_1/d_1}-1)+1]+H_1e^{r_1/d_1}r_1\}\\&\quad\times d_2{r_2}^{5/2}[H_2(e^{r_2/d_2}-1)+1]^{5/2}\\&\quad=Z_{eff2}^{3/2}\{d_2[H_2(e^{r_2/d_2}-1)+1]\\&\qquad+H_2e^{r_2/d_2}r_1\}d_1{r_1}^{5/2}[H_1(e^{r_1/d_1}-1)+1]^{5/2},\\&\qquad r=r_1+r_2,\end{aligned} \tag{8}$$

where Z_{eff1} and Z_{eff2} are the effective nuclear charges for the Ar ion and Au atom, respectively. $H_1=2.677$, d_1

$=0.862$, $H_2=3.753$, and $d_2=0.657$ can be found in Ref. [28] describing the potential of two colliding partners.

It has been pointed out by several authors [31,32] that the physical state of the target atom does not have a perceptible effect on energy loss. Within the framework of this model, we assume that the change of populations in different shells of the target atom is negligible. The populations in the Au atom are therefore set to the ground state and do not vary during the interaction. For the Ar ion, the time evolution of the populations of different shells is described by a neutralization model [12,13] mentioned below. Here only a short overview of the model is given.

It is assumed that the major process responsible for the neutralization is electron capture into Ar M, N, and O shells during the approach to the surface. The capture process is known as ''side feeding'' [24,25,33,34]. The capture rates Γ_n^{SF} $(n=M,N,O)$ are described by a function that exponentially decays with the distance to the surface [9]. The direct capture into the L shell is excluded in the simulation (i.e., $\Gamma_L^{SF}=0$) due to the large energy level mismatch (of, e.g., about 160 eV between $2p$ of Ar and $4f$ of Au). The capture rates contain three fitting parameters Γ_{n0}^{SF} for the M, N, and O shells. These parameters are determined by the comparison of the mean outgoing charge state $\overline{Q}$ between the experiments and simulations. The electron capture into higher n states is represented by the O shell. The contribution of high-n states to neutralization is small due to the fact that Auger cascades are rather slow, typically in the 10^{-14}-sec time scale for each step [35,36].

During the approach to the surface, the potential barrier between the ion and surface drops. The inner-shell levels of Ar below the conduction band are shifted upward due to the image interaction. Electrons from N and higher shells are lost into the conduction band of the solid or into empty states above the Fermi edge. For simplicity, we describe the electron loss by completely depleting the shells when the distance r between the incoming ion and the crystal surface gets smaller than the shell radius R_n. Coster-Kronig transitions within the subshells are not included. Furthermore, since transition probabilities for radiative deexcitation are at least two orders of magnitude smaller than those of Auger processes, the radiative deexcitation is omitted in the present model.

The time-dependent populations ω_n(t) in different shells for Ar ions are obtained by numerically solving the rate equations along the ion trajectory [12]. For $R_n<r$,

$$\frac{d\omega_O(t)}{dt}=\Gamma_O^{SF}-\Gamma_{LMO}-\Gamma_{LNO}-\Gamma_{MNO}-2\Gamma_{LOO}-2\Gamma_{MOO}-2\Gamma_{NOO},$$

$$\frac{d\omega_N(t)}{dt}=\Gamma_N^{SF}+\Gamma_{NOO}-\Gamma_{LMN}-2\Gamma_{LNN}-\Gamma_{LNO}-2\Gamma_{MNN}-\Gamma_{MNO},$$

$$\frac{d\omega_M(t)}{dt}=\Gamma_M^{SF}+\Gamma_{MNN}+\Gamma_{MNO}+\Gamma_{MOO}-2\Gamma_{LMM}-\Gamma_{LMN}-\Gamma_{LMO},$$

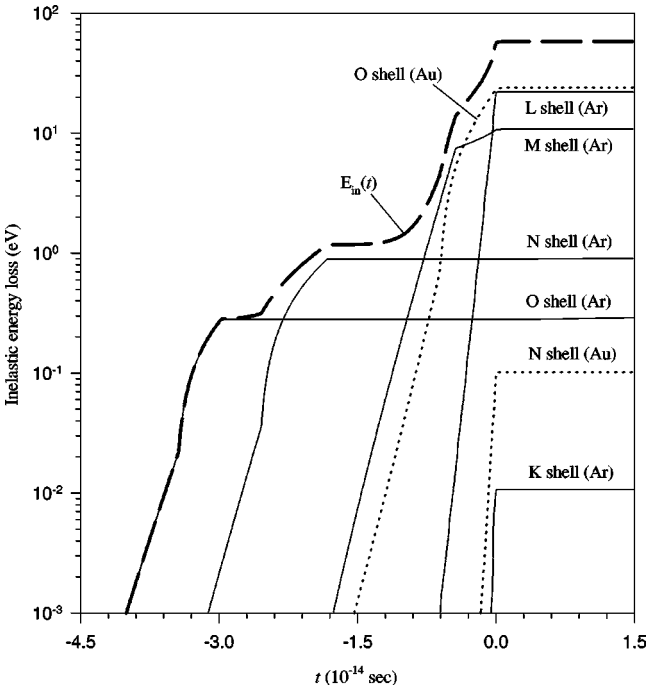

FIG. 2. Time evolution of the inelastic energy loss of Ar^{9+} ion during interaction with Au atoms on the surface ($\psi=5°$, $\theta=75°$) as predicted by a modified Firsov model including electron capture, recapture, and Auger transitions.

$$\frac{d\omega_L(t)}{dt}=\Gamma_L^{SF}+\Gamma_{LMM}+\Gamma_{LMN}+\Gamma_{LMO}+\Gamma_{LNN}+\Gamma_{LNO}+\Gamma_{LOO}.$$

For $R_{n'}\geq r$,

$$\omega_{n'}(t)=0, \tag{9}$$

where $n=L,M,N,O$ and $n'=N$ and O are the indices representing the L, M, N, and O shells of Ar. We follow the convention of the indices used in Auger rates, e.g., Γ_{LMM} describes the rate for LMM Auger transitions, i.e., one electron drops from the initial M shell to the L shell and another electron in the same M shell is ejected (with an analogous description for the others). The Auger transition rates needed to solve the rate equations are extrapolated from known transition rates by semiempirical expressions that average specific shell and subshell populations previously used in Ref. [12]. The initial populations for the shells are set to the ground states. The projectile motion is approximated by two straight-line trajectories with constant velocities obtained from the experiment. The total flight time (about 1 μsec) used in the simulation is estimated according to the geometry of the experimental setup.

The inelastic energy loss is evaluated by summing up the contributions of different shells in each individual collision for the two colliding partners and then adding up the contributions for all collisions the ion experiences along its trajectory. An average distance a of $a=5.5$ a.u. for two neighboring Au atoms along the ion trajectory is used in the simulation.

In Figs. 2 and 3 we present the time evolution of the inelastic energy loss and the electron population number

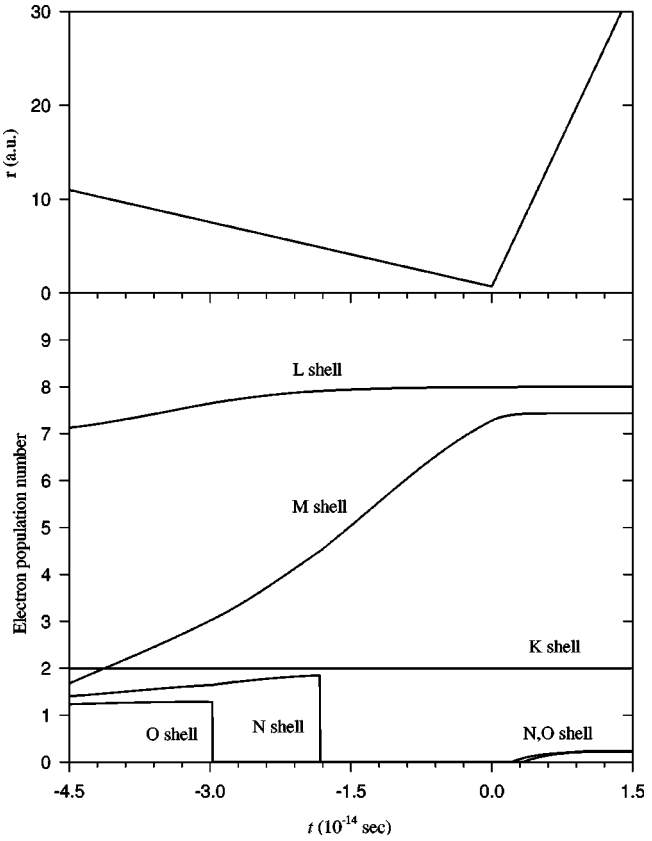

FIG. 3. Time evolution of the *K*-, *L*-, *M*-, *N*-, and *O*-shell electron population numbers for Ar^{9+} scattered from a Au(111) surface with $\psi=5°$ and $\theta=75°$ (lower part). The corresponding ion trajectory is shown in the upper part.

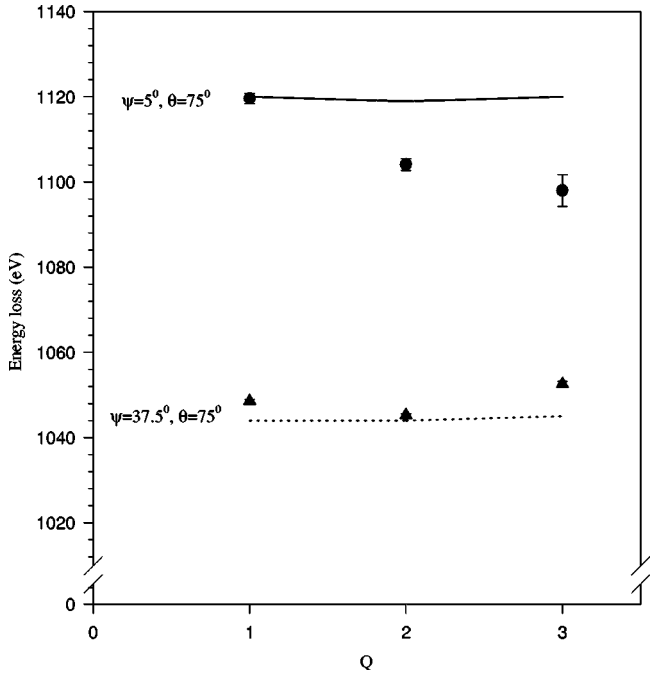

FIG. 4. Energy loss of Ar ions scattered by an angle of $\theta=75°$ from a Au(111) surface plotted as a function of the outgoing charge state Q. The data for two different incident angles $\psi=5°$ (dots) and 37.5° (triangles) are compared to the energy loss obtained from the model simulation represented by the solid line and dotted line, respectively.

variation simulated for 4-keV Ar^{9+} on Au with $\psi=5°$, $\theta=75°$. For clarity, the ion trajectory is also included. Time zero is selected at the distance of closest approach to the crystal surface. The fitting parameters Γ_{n0}^{SF} used in the simulation were derived from the measured mean outgoing charge state ($\overline{Q}=0.33\pm0.10$). With $\overline{Q}=0.33$ we obtained $\Gamma_{n0}^{SF}=4.1\times10^{-3}$ $(n=M,N,O)$, which is close to the values in Refs. [9,12]. Using this parameter, the model predicts a total inelastic energy loss of $E_{in}=58$ eV for $\psi=5°$.

As shown in Fig. 2, the inelastic energy loss increases steadily when the ion approaches the surface. The contribution from the outgoing trajectory is rather small. This is due to an almost completely deexcited projectile when it reaches the distance of closest approach to the surface as shown in Fig. 3. Nearly 95% of the vacancies in the Ar ion are already filled on the incoming way terminating flux of electron density between the ion and target atoms. Therefore, the increase of inelastic energy loss is stopped on the outgoing trajectory.

The different, shell-specific contributions to the inelastic energy loss along the ion trajectory are also shown in Fig. 2. When the distance to the surface is large ($r>5$ a.u.), inelastic energy loss is mainly due to flux to high-*n* states in the Ar ion (e.g., higher than the *O* and the *N* shell). The flattening after the rapid increase in the inelastic energy loss (see Fig. 2) can be directly correlated to the fast filling and recapture in high-*n* states. One can see that the recapture process is very important because it opens the possibility for flux into inner shells of the ion during the close interactions. The contributions of outer shells (e.g., the *O* and *N* shells) to the inelastic energy loss are rather small (around 1 eV). This is due to a weak overlap of wave functions between the ion and Au atoms because of the large impact parameters. Significant contributions to inelastic energy loss from flux to inner shells occur at close interactions ($r<5$ a.u.).

V. DISCUSSION

Figure 4 shows the measured energy loss as a function of outgoing charge states for both incident angles of $\psi=5°$ (circles) and $\psi=37.5°$ (triangles) together with the calculated energy loss E_{total} as a full line and dashed line, respectively. This plot shows again clearly the different energy losses for different incident angles at the same scattering angle of $\theta=75°$. One can see that the simulation results are in fair agreement with the experimental data for the large incident angle of 37.5°. The model predicts an energy loss that is only slightly lower than that obtained from the experiment (see also values in Table I). If we neglect a dependence on the outgoing charge state, the predicted average energy loss of $E_{total}=1044$ eV agrees with the experimental mean value of 1048.8 ± 0.8 eV.

In the case of a small incident angle of $\psi=5°$ good absolute agreement is obtained only for $Q=1+$. An increasing discrepancy between the experimental data and the model simulation is found for increasing outgoing charge states. The energy loss calculated by the model can not reproduce the experimental results of a decreasing energy loss with increasing Q. This has to be due to a simplification in the model. A disregard of the plasmon excitation, however,

cannot be used to explain this discrepancy. Plasmon excitation results in an increase of inelastic energy loss with incoming and outgoing charge states. Since the experimental value of energy loss is already lower than that calculated by the model a strong contribution of plasmon excitation would increase the discrepancy.

It is clear that the simplifications of the neutralization process in the model cannot give an inelastic energy loss dependent on the outgoing charge state. First, the present model treats the neutralization with average population numbers in the shells. In order to study quantitatively the behavior of E_{in} with different Q, an individual shell-dependent population should be taken into consideration. Second, in the present model we simplify the ion trajectories by straight lines determined only by the large-angle single scattering event. The small-angle scattering events and therefore also the energy loss are much more dependent on the degree of neutralization because of the variation in the screening and consequently the interaction potential. The trajectories vary according to the degree of neutralization and therefore also E_{in}. It is, however, still an open question where the outgoing charge state is determined: by a statistical process on the outgoing trajectory or by different scattering trajectories. The variation of the energy loss with the outgoing charge states Q favors quite clearly the latter one.

VI. CONCLUSION

The angle and outgoing charge-state-dependent energy loss of 4-keV Ar^{9+} ions interacting with the Au(111) surface was investigated. Our investigation has shown a number of interesting features. First, inelastic energy loss has been found for large-angle scattering, which can be correlated to neutralization processes and availability of inner-shell vacancies during a close interaction. Second, the simulations of inelastic energy loss process using the modified Firsov model by including the processes of electron capture, recapture, and Auger transitions are in good agreement with the experimental results, which reveals that energy loss is strongly dependent on neutralization processes when ions approach and scatter from the surface. Third, a variation of the inelastic energy loss with the outgoing charge state of the scattered ions is found. This suggests that the outgoing charge state is determined already on the incoming part of the scattering trajectory.

ACKNOWLEDGMENTS

We would like to thank L. Hägg for many helpful discussions. This research was supported by the Human Capital and Mobility Program under Contract No. CHRT-CT93-0103.

[1] A. Arnau, F. Aumayr, P.M. Echenique, M. Grether, W. Heiland, J. Limburg, R. Morgenstern, P. Roncin, S. Schippers, R. Schuch, N. Stolterfoht, P. Varga, T.J.M. Zouros, and HP. Winter, Surf. Sci. Rep. **27**, 113 (1997), and references therein.

[2] M. Delaunay, M. Fehringer, R. Geller, D. Hitz, P. Varga, and HP. Winter, Phys. Rev. B **35**, 4232 (1987).

[3] N. Stolterfoht, A. Arnau, M. Grether, R. Köhrbrück, A. Spieler, R. Page, A. Saal, J. Thomaschewski, and J. Bleck-Neuhaus, Phys. Rev. A **52**, 445 (1995).

[4] E.D. Donets, Phys. Scr. **T3**, 11 (1983); E.D. Donets, Nucl. Instrum. Methods Phys. Res. B **9**, 522 (1983).

[5] J.P. Briand, L. de Billy, P. Charles, S. Essabaa, P. Briand, R. Geller, J.P. Desclaux, S. Bliman, and C. Ristori, Phys. Rev. Lett. **65**, 159 (1990).

[6] S.T. de Zwart, T. Fried, U. Jellen, A.L. Boers, and A.G. Drentje, J. Phys. B **18**, L623 (1985).

[7] L. Folkerts, S. Schippers, D.M. Zehner, and F.W. Meyer, Phys. Rev. Lett. **74**, 2204 (1995).

[8] F.W. Meyer, L. Folkerts, and S. Schippers, Nucl. Instrum. Methods Phys. Res. B **100**, 366 (1995).

[9] S. Winecki, C.L. Cocke, D. Fry, and M.P. Stöckli, Phys. Rev. A **53**, 4228 (1996).

[10] Q. Yan, D.M. Zehner, and E.W. Meyer, Phys. Rev. A **54**, 641 (1996).

[11] S. Winecki, M.P. Stöckli, and C.L. Cocke, Phys. Rev. A **56**, 538 (1997).

[12] W. Huang, H. Lebius, R. Schuch, M. Grether, and N. Stolterfoht, Phys. Rev. A **56**, 3777 (1997).

[13] W. Huang, H. Lebius, R. Schuch, M. Grether, A. Spieler, and N. Stolterfoht, Nucl. Instrum. Methods Phys. Res. B **135**, 336 (1998).

[14] R. Herrmann, C.L. Cocke, J. Ullrich, S. Hagmann, M. Stoeckli, and H. Schmidt-Boecking, Phys. Rev. B **50**, 1435 (1994).

[15] T. Schenkel, M.A. Briere, A.V. Barnes, A.V. Hamza, K. Bethge, H. Schmidt-Boecking, and D.H. Schneider, Phys. Rev. Lett. **79**, 2030 (1997); T. Schenkel, A.V. Hamza, A.V. Barnes, and D.H. Schneider, Phys. Rev. A **55**, R1701 (1997).

[16] S. Winecki, M.P. Stöckli, and C.L. Cocke, Phys. Rev. A **55**, 4310 (1997).

[17] I.G. Hughes, J. Limburg, R. Hoekstra, R. Morgenstern, S. Hustedt, N. Hatke, and W. Heiland, Nucl. Instrum. Methods Phys. Res. B **98**, 458 (1995).

[18] H. Niehus, W. Heiland, and E. Taglauer, Surf. Sci. Rep. **17**, 213 (1993).

[19] A. Itoh, T. Schneider, G. Schiewits, Z. Roller, H. Platten, G. Nolte, D. Schneider, and N. Stolterfoht, J. Phys. B **16**, 3965 (1983).

[20] M. Grether, D. Niemann, A. Spieler, and N. Stolterfoht, Phys. Rev. A **56**, 3794 (1997).

[21] H. Lebius, W. Huang, H. Gao, R. Schuch, S. Datz, and M. Benis (unpublished).

[22] H. Goldstein, *Classical Mechanics* (Addison-Wesley, Reading, MA, 1980).

[23] J. Burgdörfer, P. Lerner, and F.W. Meyer, Phys. Rev. A **44**, 5674 (1991).

[24] J. Burgdörfer, *in Review of Fundamental Processes and Applications of Atoms and Ions*, edited by C. Lin (World Scientific, Singapore, 1993).

[25] J. Burgdörfer, C. Reinhold, and F.W. Meyer, Nucl. Instrum. Methods Phys. Res. B **98**, 415 (1995).

[26] H. Winter, C. Auth, R. Schuch, and E. Beebe, Phys. Rev. Lett. **71**, 1939 (1993).

[27] F.F. Komarov and M.A. Kumakhov, Phys. Status Solidi B **58**, 389 (1973).
[28] A.E.S. Green, D. Sellin, and A. Zachor, Phys. Rev. **184**, 1 (1969).
[29] C. Nordling and J. Österman, *Physics Handbook* (Studentlitteratur, Lund, 1987), p. 278.
[30] M. Kumakhov and F. Komarov, *Energy Loss and Ion Ranges in Solids* (Gordon and Breach, New York, 1981).
[31] C. Snoek, W.F. Ver der Weg, R. Geballe, and P.K. Rol, Physica (Utrecht) **35**, 1 (1969).
[32] D.J. Bierman and D. Ven Vliet, Physica (Utrecht) **56**, 211 (1972).
[33] L. Folkerts and R. Morgenstern, Europhys. Lett. **13**, 377 (1990).
[34] H.J. Andrä, A. Simionovici, T. Lamy, A. Brenac, G. Lamboley, J.J. Bonnet, A. Fleury, M. Bonnefoy, M. Chassevent, S. Andriamonje, and A. Pesnelle, Z. Phys. D **21**, 135 (1991).
[35] F.W. Meyer, S.H. Overbury, C.C. Havener, P.A. Zeijlmans van Emmichoven, and D.M. Zehner, Phys. Rev. Lett. **67**, 732 (1991).
[36] F.W. Meyer, S.H. Overbury, C.C. Havener, P.A. Zeijlmans van Emmichoven, J. Burgdörfer, and D.M. Zehner, Phys. Rev. A **44**, 7214 (1991).